

Distribution Agreement

In presenting this thesis as a partial fulfillment of the requirements for a degree from Emory University, I hereby grant to Emory University and its agents the non-exclusive license to archive, make accessible, and display my thesis in whole or in part in all forms of media, now or hereafter now, including display on the World Wide Web. I understand that I may select some access restrictions as part of the online submission of this thesis. I retain all ownership rights to the copyright of the thesis. I also retain the right to use in future works (such as articles or books) all or part of this thesis.

Keita Morisaki

April 3, 2023

In-silico analysis of the novel *Caenorhabditis elegans* tropomyosin with poor actin affinity

by

Keita Morisaki

Shoichiro Ono
Adviser

Mathematics

Shoichiro Ono
Adviser

Talea Mayo
Committee Member

Shashank Shekhar
Committee Member

2023

In-silico analysis of the novel *Caenorhabditis elegans* tropomyosin with poor actin affinity

By

Keita Morisaki

Shoichiro Ono

Adviser

An abstract of
a thesis submitted to the Faculty of Emory College of Arts and Sciences
of Emory University in partial fulfillment
of the requirements of the degree of
Bachelor of Science with Honors

Mathematics

2023

Abstract

In-silico analysis of the novel *Caenorhabditis elegans* tropomyosin with poor actin affinity

By Keita Morisaki

Tropomyosin is an actin-binding protein found in fungi and metazoans, which regulates actin filament stability and actomyosin contraction. In metazoans, multiple tropomyosin isoforms are expressed, and many of them are involved in diverse actin-dependent processes in an isoform-specific manner. In mammals, more than 40 tropomyosin isoforms are produced, and point mutations in several isoforms cause cardiovascular and skeletal muscle diseases. However, many tropomyosin isoforms remain poorly characterized. To investigate the biological significance of tropomyosin isoforms, we use the nematode *Caenorhabditis elegans* as a model organism. In *C. elegans*, the *lev-11* gene is the sole tropomyosin gene that is essential for embryonic development, reproduction, and regulation of muscle contractility. The *lev-11* gene is controlled by two separate promoters and extensive alternative splicing, and previous studies have demonstrated production of six tropomyosin isoforms. We identified a novel seventh exon, E7c, of the *lev-11* gene and cloned a full-length cDNA encoding a novel low-molecular-weight tropomyosin isoform, LEV-11U that contains the E7c sequence. Interestingly, LEV-11U poorly bound to actin filaments *in vitro*, whereas other isoforms strongly bound to actin filaments. Here, I analyzed biophysical and biochemical properties of E7s of *C. elegans* tropomyosin isoforms. Fourier analysis showed that the 13th-order acidic periodicity, which is an actin-adapted periodicity, of LEV-11U is weaker than that of LEV-11T. Sequence alignment showed that not only several periodic residues were not conserved in the E7c-encoded sequence but it also contained a unique substitution that violates the periodicity. Lastly,

molecular dynamics simulations indicated that the E7c-encoded region poorly formed a stable coiled-coil structure. On the other hand, E7a and E7b formed unconventional interhelical bonds to stabilize their coiled-coil structures. These results indicate that E7c of the *C. elegans lev-11* gene encodes a peptide sequence that is both biochemically and biophysically unique as compared with the equivalent sequences of other tropomyosin isoforms.

In-silico analysis of the novel *Caenorhabditis elegans* tropomyosin with poor actin affinity

By

Keita Morisaki

Shoichiro Ono

Adviser

A thesis submitted to the Faculty of Emory College of Arts and Sciences
of Emory University in partial fulfillment
of the requirements of the degree of
Bachelor of Science with Honors

Mathematics

2023

Acknowledgements

I would like to first give the greatest gratitude to my advisor, Dr. Shoichiro Ono, for instructing me for approximately four years and taught me many important lessons to become like a scientist. I would also like to thank my Committee Members, Dr. Talea Mayo and Dr. Shashank Shekhar, for not only being considerate members but also for their great lectures! I enjoyed their classes. Moreover, I would also like to acknowledge Dr. Kanako Ono for inviting me to Ono lab. The research experience that I have undergone throughout my college years will definitely help my future career. Lastly, I would like acknowledge Dr. Hidehito Kurayanagi and Dr. Eichi Watabe for being amazing collaborators. Once again, I would like to thank all for their time and support.

Table of Contents

Chapter 1	Introduction	pp. 1-3
Chapter 2	Methods	pp. 4-6
Chapter 3	Results- Periodical analysis of the tropomyosin isoforms	pp. 7-8
Chapter 4	Results- <i>In silico</i> structural analysis of the tropomyosin isoforms	pp. 9-12
Chapter 5	Future directions	p. 13
Figures		pp. 14-23
Appendix A	Steps to obtain coiled-coil centers	pp. 24-25
Appendix B	The full sequence of LEV-11U organized in the 13 th -order periodicity	p. 26
References		pp. 27-30

Chapter 1: Introduction

Actin is a globular protein that is essential for various cellular functions, including muscle contraction, cell motility and architecture, intracellular vesicle transport, and cytokinesis (Pollard & Cooper, 2009). It undergoes a reversible process of polymerization into a filament, called F-actin, and depolymerization into monomeric subunits, called G-actins. These dynamic processes, as well as other functions of actin, are regulated by a number of actin-binding proteins (Pollard, 2016). Tropomyosin is an actin-binding protein found in fungi and animals, and its roles include regulation of actomyosin contraction, regulation of other actin-binding proteins, and stabilization of F-actin (Gunning et al., 2008; Hitchcock-DeGregori & Barua, 2017). In metazoans, multiple tropomyosin isoforms are expressed, and many of them are involved in diverse actin-dependent processes in an isoform-specific manner (Gunning & Hardeman, 2017). Especially, in mammals, more than 40 tropomyosin isoforms are produced, and point mutations in several isoforms cause cardiovascular and skeletal muscle diseases (Geeves et al., 2015; Marttila et al., 2014). However, many of the tropomyosin isoforms remain poorly characterized.

Tropomyosin forms a coiled-coil dimer, which is made of two intertwined α -helical chains. Its coiled-coil structure is maintained by heptad repeats (*a-b-c-d-e-f-g*), of which residues at positions *a* and *d* are nonpolar, those at positions *e* and *g* are oppositely charged, and those at positions *b*, *c*, and *f* are polar (Woolfson, 2023) (Fig. 1). Tropomyosin also contains conserved non-canonical residues at hydrophobic core, such as alanine clusters and charged residues, which are reported to be important for binding to F-actin by adapting to its helical structure (Singh & Hitchcock-DeGregori, 2006). In addition to these repeats, the presence of seven actin-adapted pseudo repeats, each of which spans approximately 40 amino acids, is

thought to be crucial for actin binding (Barua et al., 2013; McLachlan & Stewart, 1976). The recent advancement of cryogenic electron microscopy (cryo-EM) allows high-resolution images of actin-tropomyosin interactions (Selvaraj et al., 2023; von der Ecken et al., 2015; Yamada et al., 2020). Moreover, biophysical properties, such as structure and flexibility, and the actin-tropomyosin interactions of α skeletal muscle tropomyosin (TPM 1.1) have been extensively studied using molecular dynamics simulations (Lehman et al., 2018; Lehman et al., 2020; Li et al., 2011; Marchenko et al., 2020; Tsaturyan et al., 2022; Zheng & Wen, 2019). However, the biophysical and biochemical properties of many other tropomyosin isoforms are still not yet explored sufficiently with computational and biochemical analyses.

To investigate the biological significance of tropomyosin isoforms, we use the nematode *Caenorhabditis elegans* as a model organism. In *C. elegans*, the *lev-11* gene is the sole tropomyosin gene that is essential for stabilization of F-actin, ovarian contraction, muscle arm extension and morphology, embryonic development, sarcomeric assembly of F-actin, and regulation of muscle contractility (Barnes et al., 2018; Dixon & Roy, 2005; Kagawa et al., 1995; Lewis et al., 1980; Ono & Ono, 2004; Ono et al., 2022; Ono & Ono, 2002; Yu & Ono, 2006). The *lev-11* gene is controlled by two separate promoters and extensive alternative splicing, and previous studies have demonstrated production of six tropomyosin isoforms with two alternative seventh exons (E7a and E7b) (Anyanful et al., 2001; Barnes et al., 2018; Kagawa et al., 1995; Watabe et al., 2018). Recently, we identified a novel seventh exon, E7c, of the *lev-11* gene and successfully cloned a full-length cDNA encoding a novel low-molecular-weight tropomyosin isoform, LEV-11U, containing the E7c sequence (Ono et al., In preparation) (Fig. 2). Interestingly, LEV-11U poorly bound to actin filaments *in vitro*, whereas other isoforms strongly

bound to actin filaments (Ono et al., In preparation) (Fig. 3). Therefore, the aim of my research is to investigate the structural and molecular impacts of the sequences encoded by the alternative exon 7s of the *C. elegans lev-11* gene on the tropomyosin functions. Here, I report that the actin-adapted acidic periodicity of LEV-11U is weaker compared to that of LEV-11U, and sequence alignment showed that several actin-binding residues were not conserved in the E7c-encoded sequence. In addition, molecular dynamics simulations showed that the formation of a hole in a partial region of E7c, suggesting that the E7c-encoded region poorly formed a stable coiled-coil structure, whereas other E7s, E7a and E7b, were stabilized via unconventional interhelical interactions. These results indicate that alternative splicing contributes to production of biochemically distinct tropomyosin isoforms.

Chapter 2: Methods

Fourier transformation with a random sequence profile correction

First, the amino acid sequences of TPM1.1 (NP_001018), LEV-11T (BAW98146.1), and LEV-11U (GenBank accession number: OQ473578) were converted into the sequences of -1, 0, and 1, where the value of -1 is assigned to all basic residues that are not at positions a or d , the value of 0 is assigned to all non-charged residues or residues at positions a and d , and the value of 1 is assigned to all acidic residues that are not at positions a or d . Note that positions a and d theoretically correspond to residue numbers that are equivalent to 1 and 4 modulo 7, respectively. Similarly, the amino acid sequences of TPM1.1, LEV-11T, and LEV-11U were converted into the sequences of 0 and 1, where the value of 0 is assigned to all non-acidic residues or residues at positions a and d , and the value of 1 is assigned to all acidic residues that are not at positions a or d . Then, discrete Fourier analyses were performed to find the intensity of the 13th-order periodicity of each sequence starting from the i th residue to the j th residue, where i and j span from 0 to 19. That is,

$$I(i, j) := \left\| \frac{1}{N - (i + j)} \sum_{k=i}^{N-j} f_k \cdot e^{\frac{2\pi i k \cdot 13}{N - (i + j)}} \right\|,$$

where f_k is a value assigned to the k th residue, and i in the exponent corresponds to an imaginary unit. The average variation of the intensities from a random protein sequence from the same amino acids composition, J , is

$$J(i, j) := \sqrt{\frac{n^4 \phi_1^4 - 2n^3 N \phi_1^2 \phi_2 + 4n^2 (N - 1) \phi_1 \phi_3 + n^2 (N^2 - 3N + 3) \phi_2^2 - nN(N - 1) \phi_4}{N^3 (N - 1)^2 (N - 2)}}.$$

Here, n is the number of non-zero-valued residues, and

$$\phi_k(i, j) := \frac{1}{n} \sum_{s \in S} f_s^k,$$

where S is the set of the non-zero-valued residues. The normalized intensity is calculated by $I(i, j)/J(i, j)$ (McLachlan & Stewart, 1976).

Sequence alignment

In addition to the LEV-11 sequences, the following tropomyosin isoform sequences were collected: *Homo sapiens*- TPM1.8 (NP_001288218), TPM1.9 (NP_001317273), TPM3.1 (NP_705935), TPM3.2 (NP_001036816), TPM4.2 (NP_003281), TPM2.1 (NP_998839), and TPM2.3 (NP_001288155); *Drosophila melanogaster*- TM1A (NP_524360), TM1J (NP_732004.1), and TM2A (NP_524361); *Crassostrea gigas*- Cra g 1 (NP_001354222.1) and Cra g 2 (NP_001295835.2); and *Ciona intestinalis*- Ctm1 (CAA45469). Each of the sequences were aligned as described by Barua (Barua et al., 2013). Then, period 6 (P6) of each sequence was compared.

Molecular dynamics simulations and analyses

CCBuilder Mk.2 (Wood & Woolfson, 2018) was used to generate structural models of parallel coiled-coiled dimers of full-length LEV-11O, LEV-11T, and LEV-11U, which were then truncated into exon-7-encoded regions, residues 188-234 for LEV-11O (E7a) and residues 160-206 for LEV-11T (E7b) and LEV-11U (E7c). Using Visual Molecular Dynamics (VMD) (Humphrey et al., 1996), each of these structures was solvated by a rectangular box of water particles and ionized at 0.1 M KCl. The layer of the box was set to 15 Å. Nanoscale Molecular Dynamics (NAMD) was used to perform simulations with the Chemistry at Harvard Macromolecular Mechanics 36

(CHARMM36m) force fields (Huang et al., 2017), the TIP3 water model (Beglov & Roux, 1994; Jorgensen et al., 1983), and the Beglov and Roux ion parameters (Beglov & Roux, 1994; Jorgensen et al., 1983). The values of switchdist, cutoff, and pairlistdist were set to 9, 10, and 11 Å, respectively. The energy of each model was first minimized by 5,000 steps, followed by three 20-ns production runs at 310 K under the periodic boundary condition and Langevin piston. For every 20 ps, residues 214-225 of LEV-11O (E7a) and residues 186-197 of LEV-11T (E7b) and LEV-11U (E7c) of the simulation products were compared with the corresponding portions of the initial energetically minimized structures along alpha carbons. Then, the average root mean squared deviation (RMSD) of every alpha carbon within the compared range was calculated. The data were tested by one-way analysis of variance with the Holm-Sidak method for multiple pairwise comparison (Cardillo, 2023).

The presence of hydrogen bonds was examined during the production runs. Given two atoms, one acceptor, A, and one donor, D, with a hydrogen, H, when the distance between A and D and the smaller angle formed by D-H-A were less than 3.0 Å and 20 degrees, respectively, the hydrogen bond between A and D was counted as present.

The centers of a coiled-coiled structure were computed by following the definition provided by the program TWISTER (Strelkov & Burkhard, 2002). See the steps in Appendix A. In addition, as defined by Nitnai et al., the Local Bending Angle (LBA), which is the angle formed by $C^{n-7}-C^n-C^{n+7}$, was calculated to measure the bending angle of the n th center (Nitnai et al., 2007).

Chapter 3: Results- Periodical analysis of the tropomyosin isoforms

LEV-11U shows a weaker 13th-order acidic periodicity compared to LEV-11T.

The previous Fourier analyses done by McLachlan and Stewart showed that the strong intensity of acidity was obtained for the 14th-order periodicity. This periodicity of approximately 19 amino acids, is thought to be an actin-adapted periodicity because (1) high molecular-weight (HMW) isoforms, like TPM1.1, span seven actin subunits of F-actin, and (2) it is thought that there are two major actin-binding sites per actin subunit (McLachlan & Stewart, 1976). On the other hand, low molecular-weight (LMW) isoforms are composed of 256 amino acids, which make them 26 amino acids shorter than HMW isoforms. Here, to accommodate the difference in the lengths, I analyzed the 13th-order periodicities of LEV-11T and LEV-11U with truncation(s) from both termini (Fig. 4). First, when the basicity and acidity are considered simultaneously, the strongest peak for the 13th-order periodicity for TPM1.1 is 6.17 at $(i, j) = (19, 9)$ (Fig. 4A). However, without the consideration of basic residues, the intensity rises to 8.65 with the same truncations (Fig. 4B). Here, a truncation of 19 amino acids from the N-terminus is most likely required to adjust to the 13th-order periodicity. These results support the studies that the basicity of TPM1.1 does not contribute to the 14th-order periodicity. Interestingly, the truncations of the terminal residues result in the length of 256 amino acids, which is exactly the same length as that of low molecular-weight (LMW) mammalian isoforms. These results also suggest that mammalian LMW isoforms are already optimized for the 13th-order acidic periodicity. As expected, the strongest peaks of LEV-11T are 7.99 at $(i, j) = (0, 1), (1, 0)$, whereas the strongest peaks of LEV-11U were 6.80 with the same truncations (Fig. 4C, 4D).

These truncations suggest that the 13th-order periodicity is already optimized for the *C. elegans* LMW isoforms. In addition, since the only difference in sequences between LEV-11T and LEV-11U is the selection of E7s, the lower intensity in LEV-11U compared to that in LEV-11T indicates that E7c decreases the overall intensity of the 13th-order periodicity.

D181 is a unique substitution opposed to the actin-adapted periodicity.

The analyses of the residues that violate the 14th-order periodicity were previously done by Barua et al. In their study, they organized the sequence of TPM1.1 into seven periods of approximately 40 amino acids and found out that periodically appearing acidic and basic residues in the first-half of every period as actin-binding sites using alanine mutagenesis (Barua et al., 2013). Using the same organization method, I found that E7 of LEV-11s spans the first half of the sixth period (P6) (See Appendix B). In P6, there are five residues of LEV-11U that are expected to be involved in the 14th-order periodicity: R177, D181, Q185, N191, and E195. Out of these residues, three residues, D181, Q185, and N191, violate the periodicity; D181 is expected to be hydrophobic, Q185 is expected to be basic, and N191 is expected to be acidic. However, two of these violations (Q185 and N191) occur in other tropomyosin isoforms (Fig. 5). For example, aspartic acid is observed instead of a basic residue at position 185 in *H. sapiens* TPM2.1 and *C. gigas* Cra g 1, and glycine is observed instead of an acidic residue at position 191 in *Ciona intestinalis* Ctm 1 (Fig. 5). These violations suggest that Q185 and N191 may not be critical for actin affinity. However, D181 seems to be the unique substitution for E7c that violates the periodicity among the examined tropomyosin isoforms. These results suggest that the hydrophobicity or basicity is critical at position 181 for actin binding.

Chapter 4: Results- In silico structural analysis of the tropomyosin isoforms

The probabilities of forming coiled-coil structure differ among E7s.

In most high molecular-weight (HMW) isoforms, D137(*d*) is reported to be a non-canonical residue that is well conserved throughout the evolution. E218, located at position *a* of a heptad, is reported to be another noncanonical residue that is evolutionarily conserved (Barua et al., 2013). However, biophysical properties around E218 are not yet fully understood (Nitanai et al., 2007). In *C. elegans*, E218, or E190 for low molecular-weight isoforms, is present in Exon 7s, and the program COILS predicted that the probabilities of the E218/E190-containing heptad forming a coiled-coil structure are different among Exon 7s (Barnes et al., 2018; Lupas et al., 1991). I compared coiled-coil probabilities of all three exon 7s and found that E7c was predicted to have the lowest probability of forming a coiled-coil structure at this specific heptad (Fig. 6).

E7c contains a region that significantly deviates from the coiled-coiled structure.

To analyze the coiled-coil structures of E7s, molecular dynamics simulations were run for 20 ns in total of three times for each E7 using NAMD (Fig. 7A, 7B). The deviations of E190 from the energetically minimized coiled-coil structure, measured by RMSD, were 1.2 ± 0.2 Å for E7a, 1.39 ± 0.05 Å for E7b, and 2.1 ± 0.1 Å for E7c. The Holm-Šídák method shows statistically significant differences among E7s (Fig. 7C). It is important to note that E7c has the largest deviation, forming a gap within the hydrophobic core from L186 to L197 (Fig. 7B). These results support the prediction that the low probability of forming the coiled-coil structure for E7c and suggest that the biophysical property around E190 may vary by exons.

The local bending angles at E190 do not differ among E7s.

Although the traditional coiled-coil structure is a rod-like structure, tropomyosin requires local bending throughout the structure in order to bind F-actin. Many studies have suggested that D137(*d*) imparts flexibility of tropomyosin due to having a charged residue where a hydrophobic core is typically formed. This destabilization allows tropomyosin to bend its structure (Matyushenko et al., 2018; Moore et al., 2011; Sumida et al., 2008). Local bending angle (LBA), which is an angle formed by three centers of the coiled-coil structure, was introduced by Nitnai et al. to measure structural bendings. The experimental LBA at Y214-E218-Y221 of the C-terminal segment of TPM 1.1 with an extension of leucine-zipper sequence of GCN4 at its N terminus was about 9 degrees (Nitnai et al., 2007).

To understand the relationship between biochemical and biophysical properties around E190 in E7c, LBAs at several different locations were compared. The LBAs at L183-E190-L197 of E7a, E7b, and E7c were 174 ± 3 degrees, 174 ± 3 degrees, and 173 ± 4 degrees, respectively. Thus, there is no overall statistical significance of a difference in LBAs at E190 among E7s. However, in one of the three simulations for E7c, a significant increase in the LBA was observed. The presence of hydrogen bonds crossing E190 (e.g. Q187-N191 and Q188-D192) were plotted together (Fig. 8). The constant formation of the hydrogen bond within the backbone of E190 and C194 was observed for both strands throughout the production run (Fig. 8B). On the other hand, the backbone hydrogen bonds between Q187-N191 and between Q188-D192 vanished completely at approximately 17 ns for one strand, while they remain forming for the other. Beyond this point, the LBA increased from around 6.39 degrees, the average LBA from 0 ns to

17 ns, to 22 degrees, the average LBA from 17 ns to 20 ns (Fig. 8C, 8D). The 20-ns extension of this particular simulation showed that it took approximately 8 ns to readopt its α helicity for the first time and returned to the average LBA of 7.44 degrees for approximately 8 ns, followed by another alternation of the increase and decrease in LBA for 3 ns (data not shown). This shows that the excessive bending is transient but may be frequent after the initial excessive bending. Perhaps this bending may be observed more frequently in an actin-bound state. Although the reason for this bending is not understood, the bending may be introduced by S193 (*d*), as it is one of the important residues for bending α -helical protein structures in membrane proteins (Ballesteros et al., 2000). Another potential reason may be that the formation of the stable α helix for one of the strands may destabilize the other due to electrostatic repulsion between E189 and E190.

E218/E190 contributes to the stabilization of the structure of E7a/E7b but not to E7c.

As opposed to the previous understanding of the function of D137, the recent study done by Lehman et al. suggests that D137 does not contribute to flexibility but rather contributes to a twist into the structure to optimize the interactions with F-actin (Lehman et al., 2018). The twist was introduced by the interaction between D137 and R133, which is a nonconventional intrastrand interaction between positions *g* and *d*. Here, I found unconventional interstrand interactions that are present in E7a and E7b but absent in E7c (Fig. 9). In E7a, the hydrogen bond between K217(*g*) and E218(*a*) formed $36\pm 3\%$ of the time. Similarly, the hydrogen bond between R189(*g*) and E190(*a*) in E7b formed $81\pm 6\%$ of the time. E7b has a higher hydrogen bond occupancy mostly likely due to R189-E190 being able to form up to two bonds. In addition

to the R189-E190 interaction, the hydrogen bond between E190(*a*) and Y193(*d*) formed $40\pm 10\%$ of the time. Note that this interaction was absent in E7a due to having a hydrophobic residue, F211(*d*), instead. On the other hand, since E7c contains E189(*g*) and E190(*a*), the electrostatic repulsion does not allow the formation of unconventional hydrogen bonding. Moreover, the hydrogen bonding occupancy between E190(*a*) and S193(*d*) was insignificant ($2\pm 4\%$). It is most likely due to the short sidechain of serine in E7c. Overall, unlike E190 in E7c that does not form any hydrogen bonding, the interhelical interactions of E190 in E7a and E7b are most likely to contribute to the stabilization of their structures.

In TPM 1.1, several computational studies have predicted several residues around E218, such as K213, D219, E222, to be actin-binding residues (Doran et al., 2020; Lehman et al., 2018; Li et al., 2011). Similar to the newly revealed function of D137, since a basic residue, either K or R, appears at residue 217(*g*) in many isoforms, the unconventional bonding and structure induced by E218/E190 may facilitate the interaction with F-actin. Moreover, recent studies have suggested that E218 is also one of the actin-binding residues (Marchenko et al., 2020; Tsaturyan et al., 2022). However, unlike E218/E190 in E7a/E7b, E190 in E7c does not function in a similar manner, indicating that the lack of such functions may cause the unusual poor actin affinity.

Chapter 5: Future directions

In conclusion, I observed using *in-silico* analyses that E7c of the *C. elegans lev-11* gene encodes a peptide sequence that is both biochemically and biophysically unique as compared with the equivalent sequences of other tropomyosin isoforms. I propose several future studies using protein biochemistry to determine these interesting characteristics. The first experiment is an alanine mutagenesis at D181 (D181A). In the study done by Barua et al., R125A, where R125 is a periodic basic residue, resulted in a decrease in actin affinity of TPM1.1 by 9 folds (Barua et al., 2013). In other words, one residue may impact global actin binding. Here, it is important to understand whether this unique periodicity-violating residue, D181, contributes to the poor actin affinity. The second experiment is a protease sensitivity assay of LEV-11 isoforms. Molecular dynamics simulations showed that E7c contains a core gap, whereas the other E7s seem to form a stabilized coiled structures for at least 20 ns. One of the extended simulations showed that a part of its helix of E7c was deformed repetitively. It is important to extend all the simulations to verify whether the formation of excessive bending is replicable and is unique to E7c. In addition, the protease sensitivity assay allows us to understand whether LEV-11U has a disrupted secondary structure that is susceptible for protease digestion as compared with the other isoforms. Finally, the third experiment is to measure the actin affinity of LEV-11U replacing with a partial sequence of E7b that may restore the coiled-coil formation. For example, it would be interesting to see whether LEV-11U will gain the actin affinity after the replacement of its sequence from E190 to Y196 with the LEV-11T sequence from E190 to Q196.

Figures

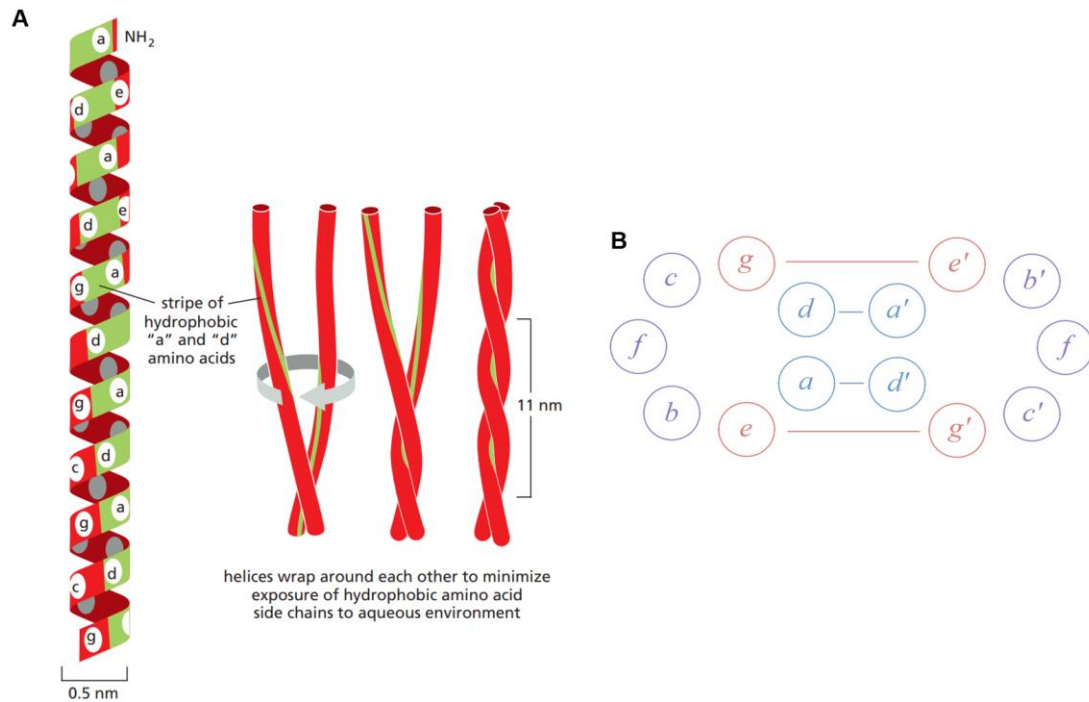


Figure 1. Coiled-coil formation requires heptad repeats. A, The formation of coiled-coil structure. Two α -helical chains, with their hydrophobic regions shown in green, form a core by hydrophobic effect (Bruce Alberts, 2014). **B,** A heptad repeat. Positions *a* and *d* (blue) are hydrophobic, positions *e* and *g* (orange) are oppositely charged, positions *b*, *c*, and *f* (purple) are polar.

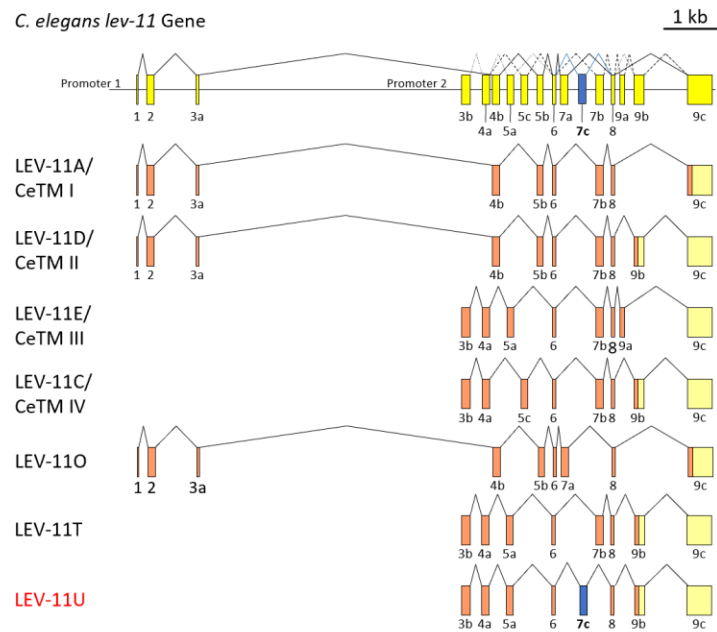


Figure 2. Exon-intron structure of the *C. elegans lev-11* gene. The top shows the schematic representation of exons (shown in boxes) and introns. Confirmed splice variants are shown below the exon-intron structure. E7c is shown in blue, and the remaining exons are in orange for coding regions and in yellow for non-coding regions. Cloning and sequencing of LEV-11U were performed by E. Watabe and H. Kuroyanagi (S. Ono, E. Watabe, K. Morisaki, K. Ono, and H. Kuroyanagi. Manuscript in preparation).

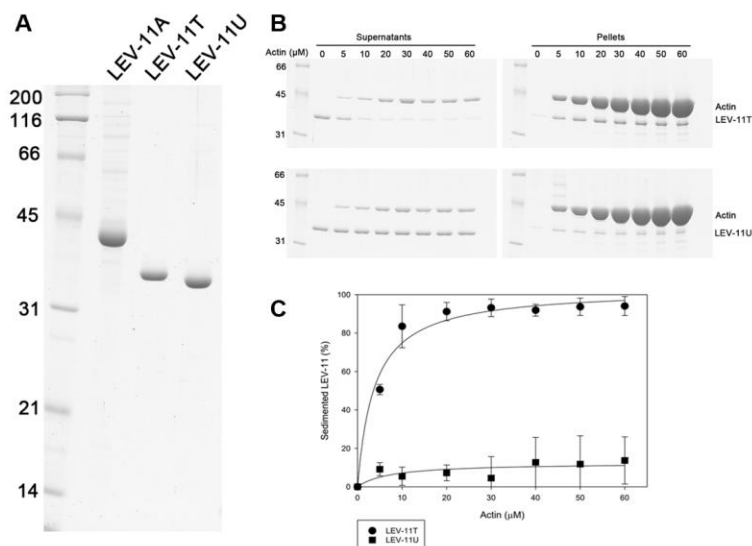


Figure 3. LEV-11U binds poorly to F-actin. **A**, Production and purification of bacterially expressed recombinant LEV-11 isoforms. LEV-11A, LEV-11T, and LEV-11U (0.5 μg each) were expressed in *E. coli* using a pET vector with no fusion tag and purified using anion exchange and hydroxyapatite column chromatography. Purified proteins were examined by SDS-PAGE and Coomassie staining. Molecular weight markers in kDa are shown on the left. **B**, F-actin co-sedimentation assay of LEV-11T and LEV-11U. A constant concentration (2 μM) of LEV-11T or LEV-11U was incubated with 0-60 μM F-actin, ultracentrifuged to separate supernatants and pellets, and analyzed by SDS-PAGE and Coomassie staining. **C**, Quantitative analysis of actin affinity of LEV-11T and LEV-11U as examined by co-sedimentation assays. LEV-11T co-sedimented with F-actin, but LEV-11U remained in the supernatants. A dissociation constant (Kd) for the binding of LEV-11T with F-actin was estimated as $3.7 \pm 0.64 \mu\text{M}$ (n=3). These

experiments were performed by S. Ono (S. Ono, E. Watabe, K. Morisaki, K. Ono, and H. Kuroyanagi. Manuscript in preparation).

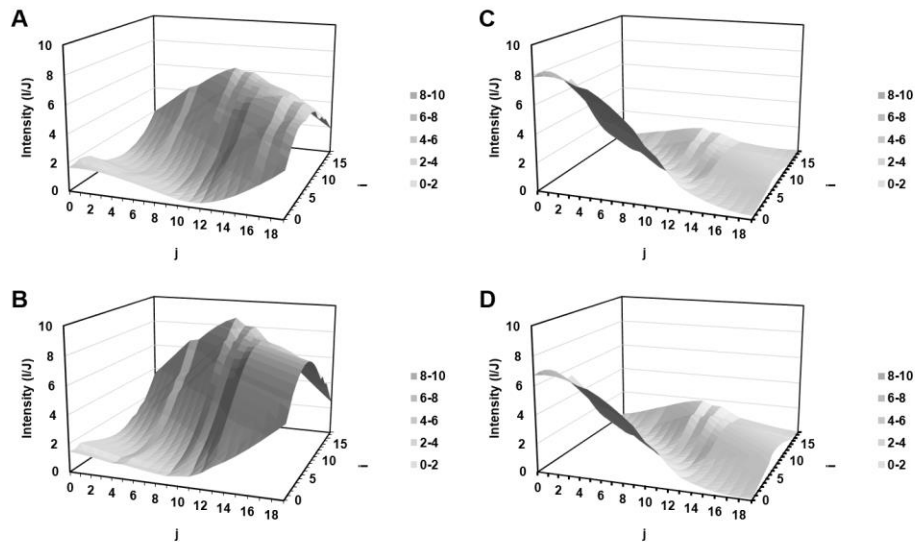


Figure 4. Fourier analysis of tropomyosin sequences. The amino acid sequence from the i th residue to the j th residue was analyzed via Fourier analysis. **A**, The graph shows the normalized intensities for the 13th-order charged periodicity of TPM1.1. **B**, The graph shows the normalized intensities for the 13th-order acidic periodicity of TPM1.1. **C**, The graph shows the normalized intensities for the 13th-order acidic periodicity of LEV-11T. **D**, The graph shows the normalized intensities for acidic periodicity of the 13th-order periodicity of LEV-11U.

Isoform	abcdefg	abcdefg	abcdefg	abcdefg	abcdefg	abcd	Species	
LEV-110	LKSLELS	EEKALEK	EDIFAEQ	IRQLDFR	LKEAETR	AEFA	<i>C. elegans</i>	
LEV-11T	LKSLEVS	EEKALQR	EDSYEEQ	IRTVSSR	LKEAETR	AEFA	<i>C. elegans</i>	
LEV-11U	177 181 185 191 195 LREAQDL	LHQ	LQQE	ENDSCEY	LNCAVES	RKEAETR	AEFA	<i>C. elegans</i>
TPM1. 8	LKSLEAQ	AEKYSQK	EDRYEEE	IKVLSDK	LKEAETR	AEFA	<i>H. sapiens</i>	
TPM1. 9	LKALMAA	EDKYSQK	EDRYEEE	IKVLSDK	LKEAETR	AEFA	<i>H. sapiens</i>	
TPM3. 1	LKCLSAA	EEKYSQK	EDKYEEE	IKILTDK	LKEAETR	AEFA	<i>H. sapiens</i>	
TPM3. 2	LKSLEAQ	AEKYSQK	EDKYEEE	IKILTDK	LKEAETR	AEFA	<i>H. sapiens</i>	
TPM4. 2	LKSLEAA	SEKYSEK	EDKYEEE	IKLLSDK	LKEAETR	AEFA	<i>H. sapiens</i>	
TPM2. 1	LKSLMAS	EEYSTK	EDKYEEE	IKLLEEK	LKEAETR	AEFA	<i>H. sapiens</i>	
TPM2. 3	LKSLEAQ	ADKYSTK	EDKYEEE	IKLLEEK	LKEAETR	AEFA	<i>H. sapiens</i>	
TM 1A	LKSLEVS	EEKATQK	EETFETQ	IKVLDSH	LKEAEAR	AEFA	<i>D. melanogaster</i>	
TM 1J	LKSLEVS	EEKANQR	EEYKNQ	IKTLNTR	LKEAEAR	AEFA	<i>D. melanogaster</i>	
TM 2A	LKSLEVS	EEKANQR	VEEFKRE	MKTLSTK	LKEAEQR	AEHA	<i>D. melanogaster</i>	
Cra g 1	MKSLEIS	EQEASQR	EDSYEET	IRDLTQR	LKDAENR	ATEA	<i>C. gigas</i>	
Cra g 2	IKTLQVQ	NDQASQR	EDSYEET	IRDLTQR	LKDAENR	ATEA	<i>C. gigas</i>	
CTm 1	LKSLEAS	AEKYAAK	EGIFEEE	IKTLSDK	LKDSETR	AEFA	<i>C. intestinalis</i>	

Figure 5. P6 of tropomyosin isoforms. The top line shows the heptad repeats with bolded letters corresponding to periodic positions. The right column shows the species that express the isoforms on the left. The blue, black, and red letters correspond to basic, non-polar, acidic residues, respectively. Residues that violate the periodicity are highlighted.

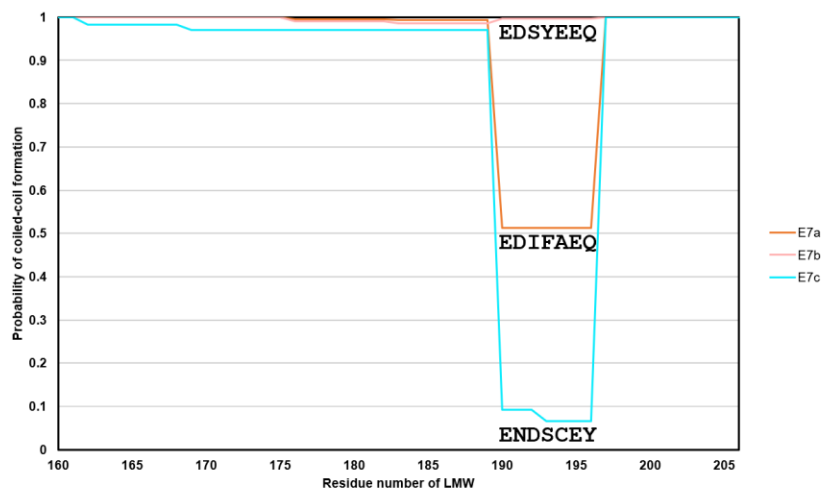


Figure 6. The probabilities of E7s forming coiled-coil structure. The program COILS predicted the probability of forming coiled-coil structure within E7s, which span from residue 160 (188) to residue 206 (234) of low (high) molecular-weight isoforms. The probability lines for E7a, E7b, and E7c are shown in orange, pink, and cyan, respectively. The heptad where the probabilities differ significantly were labeled with their respective sequences.

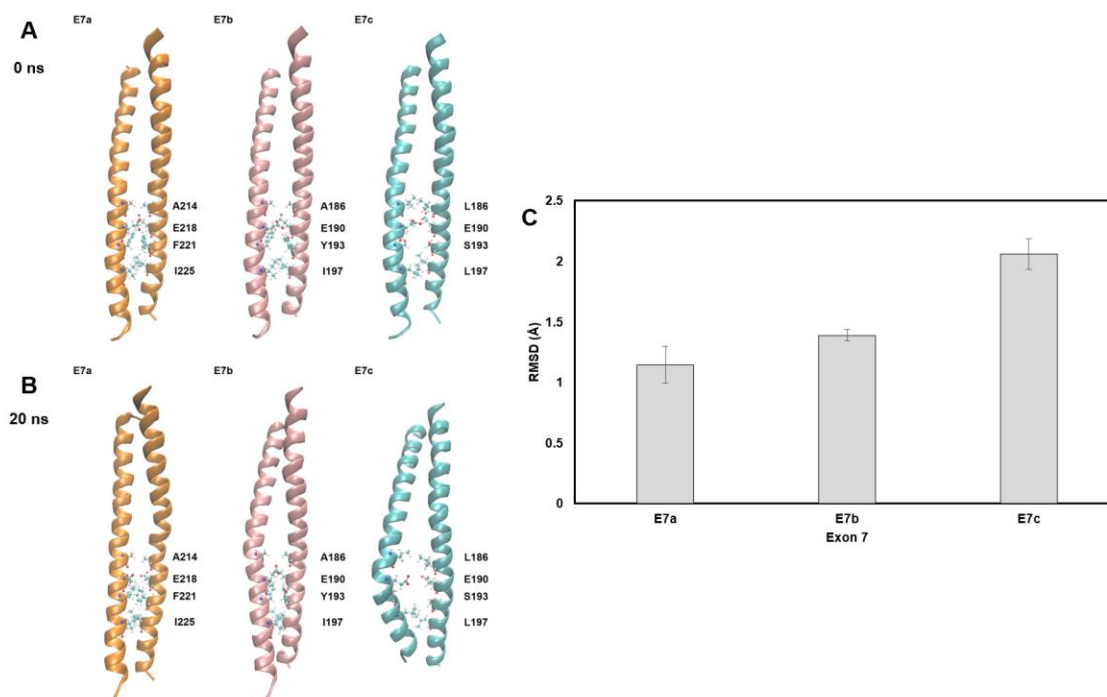


Figure 5. Molecular dynamics simulations of E7s. **A**, The initial energetically-minimized structures of E7s. The initial reference structure of E7a, E7b, and E7c are shown in orange, pink, and cyan, respectively. Several residues near E190/E218 at their respective hydrophobic cores are shown and labeled. **B**, Molecular dynamic simulations of E7s. The structures of E7a, E7b, and E7c with the most noticeable changes after simulating for 20 ns are shown in orange, pink, and cyan, respectively. Several residues at their respective hydrophobic cores are shown and labeled. **C**, The deviations from the coiled-coiled structure at E190/E218 of E7s. The average RMSDs of E7s (n=3) are shown with their respective standard deviations. The p-values of the Holm-Šídák t-tests between E7a and E7b, E7a and E7c, and E7b and E7c are $8e-05$, 0.0004, and 0.04, respectively.

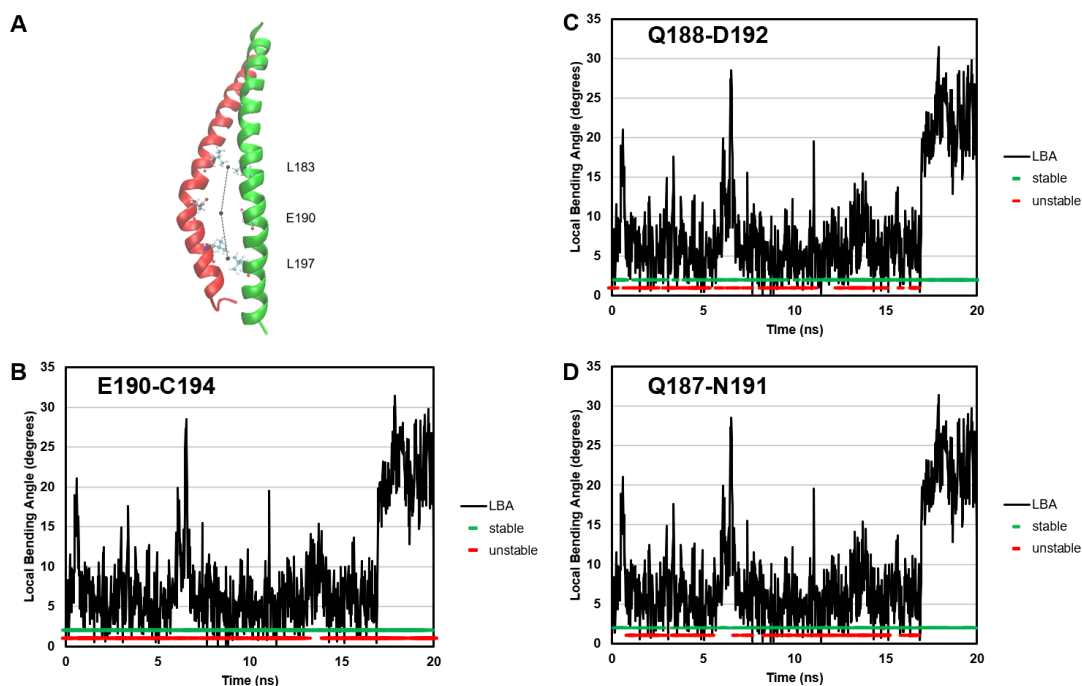


Figure 6. The analysis of local bending angle and backbone hydrogen bonding of E7c. A, The centers at position α near E190 of E7c. The centers, shown in black, of the coiled-coiled structure at L183, E190, and L197 were measured, and the angle formed by these centers (LBA) was measured. **B,** E190-C194 hydrogen bonding. LBAs are shown in black, whereas the presence of a hydrogen bonds of E190-C194 is shown in green for the stable chain and in red for the unstable chain. **C,** Q188-D192 hydrogen bonding. LBA are shown in black, whereas the presence of a hydrogen bonds of Q188-D192 is shown in green for the stable chain and in red for the unstable chain. **D,** Q187-N191 hydrogen bonding. LBA are shown in black, whereas the presence of a hydrogen bonds of Q187-N191 is shown in green for the stable chain and in red for the unstable chain. Note that the increase in LBA appeared only in one of the three runs.

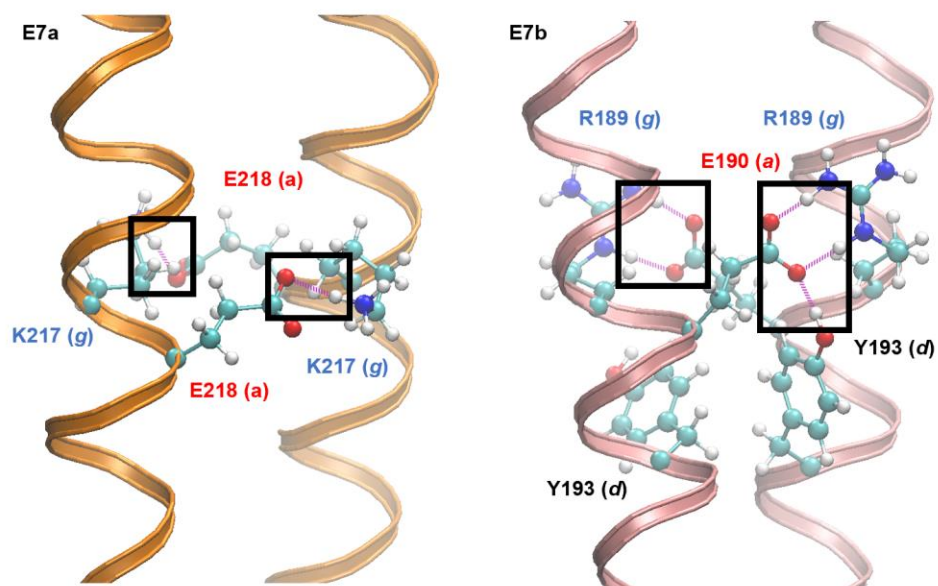


Figure 7. Unconventional hydrogen bonding in E7a and E7b. One unconventional interaction in E7a (K217(g)-E218(a)) and two unconventional interactions in E7b (R189(g)-E190(a) and E190(a)-Y193(d)) are shown. Hydrogen bonds are shown as purple dotted lines, marked with a black box. Carbon atoms, hydrogen atoms, oxygen atoms, and nitrogen atoms, are shown in cyan, white, red, and blue, respectively.

Appendix A: Steps to obtain coiled-coil centers

Consider the n th axis of a given α helix, $C_n C_{n+1}$, such that $C_n(\overrightarrow{O_n})$ and $C_{n+1}(\overrightarrow{O_{n+1}})$ are the temporal n th and $(n + 1)$ th centers of the α helix. Let the position vector of the α carbon of

the n th residue $X_n(\overrightarrow{a_n})$ be $\overrightarrow{a_n} := \begin{pmatrix} a_{1,n} \\ a_{2,n} \\ a_{3,n} \end{pmatrix}$. Then, the unit vector that is parallel to the bisector of

$\angle X_{n-1} X_n X_{n+1}$, denoted by $\overrightarrow{v_1}$, can be computed by

$$\overrightarrow{v_1} = \frac{\frac{\overrightarrow{a_{n-1}} - \overrightarrow{a_n}}{\|\overrightarrow{a_{n-1}} - \overrightarrow{a_n}\|} + \frac{\overrightarrow{a_{n+1}} - \overrightarrow{a_n}}{\|\overrightarrow{a_{n+1}} - \overrightarrow{a_n}\|}}{\left\| \frac{\overrightarrow{a_{n-1}} - \overrightarrow{a_n}}{\|\overrightarrow{a_{n-1}} - \overrightarrow{a_n}\|} + \frac{\overrightarrow{a_{n+1}} - \overrightarrow{a_n}}{\|\overrightarrow{a_{n+1}} - \overrightarrow{a_n}\|} \right\|} := \begin{pmatrix} v_{11} \\ v_{12} \\ v_{13} \end{pmatrix}.$$

Similarly, the unit vector that is parallel to the angle bisector of $\angle X_n X_{n+1} X_{n+2}$, denoted by $\overrightarrow{v_2}$, can be computed by

$$\overrightarrow{v_2} = \frac{\frac{\overrightarrow{a_n} - \overrightarrow{a_{n+1}}}{\|\overrightarrow{a_n} - \overrightarrow{a_{n+1}}\|} + \frac{\overrightarrow{a_{n+2}} - \overrightarrow{a_{n+1}}}{\|\overrightarrow{a_{n+2}} - \overrightarrow{a_{n+1}}\|}}{\left\| \frac{\overrightarrow{a_n} - \overrightarrow{a_{n+1}}}{\|\overrightarrow{a_n} - \overrightarrow{a_{n+1}}\|} + \frac{\overrightarrow{a_{n+2}} - \overrightarrow{a_{n+1}}}{\|\overrightarrow{a_{n+2}} - \overrightarrow{a_{n+1}}\|} \right\|} := \begin{pmatrix} v_{21} \\ v_{22} \\ v_{23} \end{pmatrix}.$$

Here, we assume that $\overrightarrow{O_n O_{n+1}}$ is orthogonal to $\overrightarrow{v_1}$ and $\overrightarrow{v_2}$ and that centers C_n and C_{n+1} are on the bisectors $\angle X_{n-1} X_n X_{n+1}$ and $\angle X_n X_{n+1} X_{n+2}$, respectively. Then, there exists constants s and t such that

$$\overrightarrow{O_n} = s\overrightarrow{v_1} + \overrightarrow{a_n}, \quad \overrightarrow{O_{n+1}} = t\overrightarrow{v_2} + \overrightarrow{a_{n+1}}.$$

Also, the unit vector, $\overrightarrow{v_3}$, that is parallel to $\overrightarrow{O_n O_{n+1}}$ can be computed by

$$\overrightarrow{v_3} = \frac{\overrightarrow{v_1} \times \overrightarrow{v_2}}{\|\overrightarrow{v_1} \times \overrightarrow{v_2}\|} := \begin{pmatrix} v_{31} \\ v_{32} \\ v_{33} \end{pmatrix},$$

and there is a constant u such that

$$\overrightarrow{O_n O_{n+1}} = u \vec{v}_3.$$

From the above, the problem reduces to solving the following equation:

$$\begin{pmatrix} v_{11} & -v_{21} & v_{31} \\ v_{12} & -v_{22} & v_{32} \\ v_{13} & -v_{23} & v_{33} \end{pmatrix} \begin{pmatrix} s \\ t \\ u \end{pmatrix} = \begin{pmatrix} a_{1,n+1} - a_{1,n} \\ a_{2,n+1} - a_{2,n} \\ a_{3,n+1} - a_{3,n} \end{pmatrix}.$$

The true n th center of α helix, C_n^* , is computed by taking the midpoint of the temporal C_n s computed from the axes $C_{n-1}C_n$ and C_nC_{n+1} . Finally, the n th center of a coiled-coil structure, C^n , is taken as the midpoint of the true n th centers of the two α helices.

Appendix B: The full sequence of LEV-11U organized in the 13th-order periodicity

The following is the full sequence of LEV-11U organized in the 13th-order periodicity. The periodic basic and acidic residues are colored in blue and red, respectively.

abcdefg abcdefg abcdefg abcdefg abcdefg abcdefg abcd (heptad positions)

3b (exon #)

MSKVN**KE** GAQQTSL LDVL

4a

KKK MRQAREE **EA**AKDE ADEVKRQ LEEERKK REDAEAE VAAL

NRR IVLVEED **LE**RTEDR LKTATSK LEQATKA ADEA

5a

6

DRA RKSMETR SQQDE**ER** ANFLETQ VDEAKVI AEDADRK YEEV

7c

ARK LAMVEAD **LE**RAEER AEAGEKR SNLAEAH MRGLSVN

8

LREAQDL LHQLQ**QE** ENDS**CE**Y LNCAVES RKEAETR AEFA

9b

ERS VQKLQ**KE** VDRLE**EL** RDAEVLK ARQLQDE LDHMQE LNSV

References

- Anyanful, A., Sakube, Y., Takuwa, K., & Kagawa, H. (2001). The third and fourth tropomyosin isoforms of *Caenorhabditis elegans* are expressed in the pharynx and intestines and are essential for development and morphology. *J Mol Biol*, 313(3), 525-537.
<https://doi.org/10.1006/jmbi.2001.5052>
- Ballesteros, J. A., Deupi, X., Olivella, M., Haaksma, E. E., & Pardo, L. (2000). Serine and threonine residues bend alpha-helices in the chi(1) = g(-) conformation. *Biophys J*, 79(5), 2754-2760. [https://doi.org/10.1016/s0006-3495\(00\)76514-3](https://doi.org/10.1016/s0006-3495(00)76514-3)
- Barnes, D. E., Watabe, E., Ono, K., Kwak, E., Kuroyanagi, H., & Ono, S. (2018). Tropomyosin isoforms differentially affect muscle contractility in the head and body regions of the nematode *Caenorhabditis elegans*. *Mol Biol Cell*, 29(9), 1075-1088.
<https://doi.org/10.1091/mbc.E17-03-0152>
- Barua, B., Fagnant, P. M., Winkelmann, D. A., Trybus, K. M., & Hitchcock-DeGregori, S. E. (2013). A periodic pattern of evolutionarily conserved basic and acidic residues constitutes the binding interface of actin-tropomyosin. *J Biol Chem*, 288(14), 9602-9609.
<https://doi.org/10.1074/jbc.M113.451161>
- Beglov, D., & Roux, B. (1994). Finite Representation of an Infinite Bulk System - Solvent Boundary Potential for Computer-Simulations. *Journal of Chemical Physics*, 100(12), 9050-9063. [https://doi.org/Doi 10.1063/1.466711](https://doi.org/Doi%2010.1063/1.466711)
- Bruce Alberts, A. J., Julian Lewis, David Morgan, Martin Raff, Keith Roberts, Peter Walter. (2014). *Molecular Biology of the Cell* (6 ed.). Garland Science.
- Cardillo, G. (2023). *Holm-Sidak t-test*. In (Version 2.0.0.0) <https://github.com/dnafinder/holm>
- Dixon, S. J., & Roy, P. J. (2005). Muscle arm development in *Caenorhabditis elegans*. *Development*, 132(13), 3079-3092. <https://doi.org/10.1242/dev.01883>
- Doran, M. H., Pavadai, E., Rynkiewicz, M. J., Walklate, J., Bullitt, E., Moore, J. R., Regnier, M., Geeves, M. A., & Lehman, W. (2020). Cryo-EM and Molecular Docking Shows Myosin Loop 4 Contacts Actin and Tropomyosin on Thin Filaments. *Biophys J*, 119(4), 821-830.
<https://doi.org/10.1016/j.bpj.2020.07.006>
- Geeves, M. A., Hitchcock-DeGregori, S. E., & Gunning, P. W. (2015). A systematic nomenclature for mammalian tropomyosin isoforms. *J Muscle Res Cell Motil*, 36(2), 147-153.
<https://doi.org/10.1007/s10974-014-9389-6>
- Gunning, P., O'Neill, G., & Hardeman, E. (2008). Tropomyosin-based regulation of the actin cytoskeleton in time and space. *Physiol Rev*, 88(1), 1-35.
<https://doi.org/10.1152/physrev.00001.2007>
- Gunning, P. W., & Hardeman, E. C. (2017). Tropomyosins. *Curr Biol*, 27(1), R8-r13.
<https://doi.org/10.1016/j.cub.2016.11.033>
- Hitchcock-DeGregori, S. E., & Barua, B. (2017). Tropomyosin Structure, Function, and Interactions: A Dynamic Regulator. *Subcell Biochem*, 82, 253-284.
https://doi.org/10.1007/978-3-319-49674-0_9
- Huang, J., Rauscher, S., Nawrocki, G., Ran, T., Feig, M., de Groot, B. L., Grubmuller, H., & MacKerell, A. D., Jr. (2017). CHARMM36m: an improved force field for folded and

- intrinsically disordered proteins. *Nat Methods*, 14(1), 71-73.
<https://doi.org/10.1038/nmeth.4067>
- Humphrey, W., Dalke, A., & Schulten, K. (1996). VMD: visual molecular dynamics. *J Mol Graph*, 14(1), 33-38, 27-38. <http://www.ncbi.nlm.nih.gov/htbin-post/Entrez/query?db=m&form=6&dopt=r&uid=8744570>
- Jorgensen, W. L., Chandrasekhar, J., Madura, J. D., Impey, R. W., & Klein, M. L. (1983). Comparison of Simple Potential Functions for Simulating Liquid Water. *Journal of Chemical Physics*, 79(2), 926-935. <https://doi.org/Doi 10.1063/1.445869>
- Kagawa, H., Sugimoto, K., Matsumoto, H., Inoue, T., Imadzu, H., Takuwa, K., & Sakube, Y. (1995). Genome structure, mapping and expression of the tropomyosin gene tmy-1 of *Caenorhabditis elegans*. *J Mol Biol*, 251(5), 603-613.
<https://doi.org/10.1006/jmbi.1995.0459>
- Lehman, W., Li, X., Kiani, F. A., Moore, J. R., Campbell, S. G., Fischer, S., & Rynkiewicz, M. J. (2018). Precise Binding of Tropomyosin on Actin Involves Sequence-Dependent Variance in Coiled-Coil Twisting. *Biophys J*, 115(6), 1082-1092.
<https://doi.org/10.1016/j.bpj.2018.08.017>
- Lehman, W., Rynkiewicz, M. J., & Moore, J. R. (2020). A new twist on tropomyosin binding to actin filaments: perspectives on thin filament function, assembly and biomechanics. *J Muscle Res Cell Motil*, 41(1), 23-38. <https://doi.org/10.1007/s10974-019-09501-5>
- Lewis, J. A., Wu, C. H., Berg, H., & Levine, J. H. (1980). The genetics of levamisole resistance in the nematode *Caenorhabditis elegans*. *Genetics*, 95(4), 905-928.
<https://doi.org/10.1093/genetics/95.4.905>
- Li, X. E., Tobacman, L. S., Mun, J. Y., Craig, R., Fischer, S., & Lehman, W. (2011). Tropomyosin position on F-actin revealed by EM reconstruction and computational chemistry. *Biophys J*, 100(4), 1005-1013. <https://doi.org/10.1016/j.bpj.2010.12.3697>
- Lupas, A., Van Dyke, M., & Stock, J. (1991). Predicting coiled coils from protein sequences. *Science*, 252(5009), 1162-1164. <https://doi.org/10.1126/science.252.5009.1162>
- Marchenko, M. A., Nefedova, V. V., Yampolskaya, D. S., Kopylova, G. V., Shchepkin, D. V., Bershitsky, S. Y., Koubassova, N. A., Tsaturyan, A. K., Levitsky, D. I., & Matyushenko, A. M. (2020). Impact of A134 and E218 Amino Acid Residues of Tropomyosin on Its Flexibility and Function. *Int J Mol Sci*, 21(22). <https://doi.org/10.3390/ijms21228720>
- Marttila, M., Lehtokari, V. L., Marston, S., Nyman, T. A., Barnerias, C., Beggs, A. H., Bertini, E., Ceyhan-Birsoy, O., Cintas, P., Gerard, M., Gilbert-Dussardier, B., Hogue, J. S., Longman, C., Eymard, B., Frydman, M., Kang, P. B., Klinge, L., Kolski, H., Lochmüller, H., . . . Wallgren-Pettersson, C. (2014). Mutation update and genotype-phenotype correlations of novel and previously described mutations in TPM2 and TPM3 causing congenital myopathies. *Hum Mutat*, 35(7), 779-790. <https://doi.org/10.1002/humu.22554>
- Matyushenko, A. M., Shchepkin, D. V., Kopylova, G. V., Bershitsky, S. Y., Koubassova, N. A., Tsaturyan, A. K., & Levitsky, D. I. (2018). Functional role of the core gap in the middle part of tropomyosin. *Febs j*, 285(5), 871-886. <https://doi.org/10.1111/febs.14369>
- McLachlan, A. D., & Stewart, M. (1976). The 14-fold periodicity in alpha-tropomyosin and the interaction with actin. *J Mol Biol*, 103(2), 271-298. [https://doi.org/10.1016/0022-2836\(76\)90313-2](https://doi.org/10.1016/0022-2836(76)90313-2)

- Moore, J. R., Li, X., Nirody, J., Fischer, S., & Lehman, W. (2011). Structural implications of conserved aspartate residues located in tropomyosin's coiled-coil core. *Bioarchitecture*, 1(5), 250-255. <https://doi.org/10.4161/bioa.18117>
- Nitanai, Y., Minakata, S., Maeda, K., Oda, N., & Maéda, Y. (2007). Crystal structures of tropomyosin: flexible coiled-coil. *Adv Exp Med Biol*, 592, 137-151. https://doi.org/10.1007/978-4-431-38453-3_13
- Ono, K., & Ono, S. (2004). Tropomyosin and troponin are required for ovarian contraction in the *Caenorhabditis elegans* reproductive system. *Mol Biol Cell*, 15(6), 2782-2793. <https://doi.org/10.1091/mbc.e04-03-0179>
- Ono, S., Lewis, M., & Ono, K. (2022). Mutual dependence between tropomodulin and tropomyosin in the regulation of sarcomeric actin assembly in *Caenorhabditis elegans* striated muscle. *Eur J Cell Biol*, 101(2), 151215. <https://doi.org/10.1016/j.ejcb.2022.151215>
- Ono, S., & Ono, K. (2002). Tropomyosin inhibits ADF/cofilin-dependent actin filament dynamics. *J Cell Biol*, 156(6), 1065-1076. <https://doi.org/10.1083/jcb.200110013>
- Pollard, T. D. (2016). Actin and Actin-Binding Proteins. *Cold Spring Harb Perspect Biol*, 8(8). <https://doi.org/10.1101/cshperspect.a018226>
- Pollard, T. D., & Cooper, J. A. (2009). Actin, a central player in cell shape and movement. *Science*, 326(5957), 1208-1212. <https://doi.org/10.1126/science.1175862>
- Selvaraj, M., Kokate, S. B., Reggiano, G., Kogan, K., Kotila, T., Kremneva, E., DiMaio, F., Lappalainen, P., & Huiskonen, J. T. (2023). Structural basis underlying specific biochemical activities of non-muscle tropomyosin isoforms. *Cell reports*, 42(1), 111900. <https://doi.org/10.1016/j.celrep.2022.111900>
- Singh, A., & Hitchcock-DeGregori, S. E. (2006). Dual requirement for flexibility and specificity for binding of the coiled-coil tropomyosin to its target, actin. *Structure*, 14(1), 43-50. <https://doi.org/10.1016/j.str.2005.09.016>
- Strelkov, S. V., & Burkhard, P. (2002). Analysis of alpha-helical coiled coils with the program TWISTER reveals a structural mechanism for stutter compensation. *J Struct Biol*, 137(1-2), 54-64. <https://doi.org/10.1006/jsbi.2002.4454>
- Sumida, J. P., Wu, E., & Lehrer, S. S. (2008). Conserved Asp-137 imparts flexibility to tropomyosin and affects function. *J Biol Chem*, 283(11), 6728-6734. <https://doi.org/10.1074/jbc.M707485200>
- Tsaturyan, A. K., Zaklyazminskaya, E. V., Polyak, M. E., Kopylova, G. V., Shchepkin, D. V., Kochurova, A. M., Gonchar, A. D., Kleymenov, S. Y., Koubasova, N. A., Bershitsky, S. Y., Matyushenko, A. M., & Levitsky, D. I. (2022). De Novo Asp219Val Mutation in Cardiac Tropomyosin Associated with Hypertrophic Cardiomyopathy. *Int J Mol Sci*, 24(1). <https://doi.org/10.3390/ijms24010018>
- von der Ecken, J., Müller, M., Lehman, W., Manstein, D. J., Penczek, P. A., & Raunser, S. (2015). Structure of the F-actin-tropomyosin complex. *Nature*, 519(7541), 114-117. <https://doi.org/10.1038/nature14033>
- Watabe, E., Ono, S., & Kuroyanagi, H. (2018). Alternative splicing of the *Caenorhabditis elegans* lev-11 tropomyosin gene is regulated in a tissue-specific manner. *Cytoskeleton (Hoboken)*, 75(10), 427-436. <https://doi.org/10.1002/cm.21489>

- Wood, C. W., & Woolfson, D. N. (2018). CCBUILDER 2.0: Powerful and accessible coiled-coil modeling. *Protein Sci*, 27(1), 103-111. <https://doi.org/10.1002/pro.3279>
- Woolfson, D. (2023). Understanding a protein fold: the physics, chemistry, and biology of α -helical coiled coils. *J Biol Chem*, 104579. <https://doi.org/10.1016/j.jbc.2023.104579>
- Yamada, Y., Namba, K., & Fujii, T. (2020). Cardiac muscle thin filament structures reveal calcium regulatory mechanism. *Nat Commun*, 11(1), 153. <https://doi.org/10.1038/s41467-019-14008-1>
- Yu, R., & Ono, S. (2006). Dual roles of tropomyosin as an F-actin stabilizer and a regulator of muscle contraction in *Caenorhabditis elegans* body wall muscle. *Cell Motil Cytoskeleton*, 63(11), 659-672. <https://doi.org/10.1002/cm.20152>
- Zheng, W., & Wen, H. (2019). Molecular dynamics simulation of tropomyosin bound to actins/myosin in the closed and open states. *Proteins*, 87(10), 805-814. <https://doi.org/10.1002/prot.25707>